

π -Self-Assembly of a Coronene on Carbon Nanomaterial-Modified Electrode and Its Symmetrical Redox and H₂O₂ Electrocatalytic Reduction Functionalities

Sivakumar Nisha and Annamalai Senthil Kumar*

Cite This: *ACS Omega* 2020, 5, 11817–11828

Read Online

ACCESS |



Metrics & More

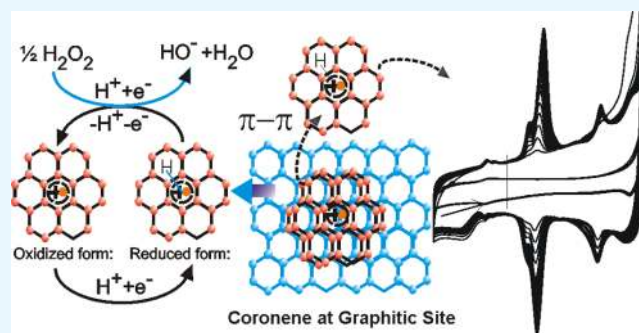


Article Recommendations



Supporting Information

ABSTRACT: The structure–electroactivity relationship of graphene has been studied using coronene (Cor), polyaromatic hydrocarbon (PAH), and a subunit of graphene as a model system by chemically modified electrode approach. In general, graphene and PAH do not show any redox activity in their native form. Herein, we report a simple electrochemical approach for the conversion of electro-inactive coronene to a highly redox-active molecule (Cor-Redox; $E^{o'} = 0.235 \pm 0.005$ V vs Ag/AgCl) after being adsorbed on graphitic carbon nanomaterial and preconditioned at an applied potential, 1.2 V vs Ag/AgCl, wherein, the water molecule oxidizes to dioxygen via hydroxyl radical ($\cdot\text{OH}$) intermediate, in acidic solution (pH 2 KCl–HCl). When the same coronene electrochemical experiment was carried out on an unmodified glassy carbon electrode, there was no sign of faradic signal, revealing the unique electrochemical behavior of the coronene molecule on graphitic nanomaterial. The Cor-Redox peak is found to be highly symmetrical (peak-to-peak potential separation of ~ 0 V tested by cyclic voltammetry (CV)) and surface-confined ($\Gamma_{\text{Cor-Redox}} = 10.1 \times 10^{-9}$ mol cm^{-2}) and has proton-coupled electron-transfer ($\partial E^{o'}/\partial \text{pH} = -56$ mV pH^{-1}) character. Initially, it was speculated that Cor is converted to a hydroxy group-functionalized Cor molecule (dihydroxy benzene derivative) on the graphitic surface and showed the electrochemical redox activity. However, physicochemical characterization studies including Raman, IR, transmission electron microscopy (TEM), X-ray photoelectron spectroscopy (XPS), redox-site selective oxidation probe, cysteine (for dihydroxy benzene), radical scavenger ((2,2,6,6-tetramethylpiperidin-1-yl)oxyl, TEMPO), and scanning electrochemical microscopy (SECM) using ferricyanide redox couple have revealed that coronene cationic radical species like electroactive molecule is formed on graphitic material upon the electrochemical oxidation reaction at a high anodic potential. It has been proposed that $\cdot\text{OH}$ generated as an intermediate species from the water oxidation reaction is involved in the coronene cationic radical species. Studies on coronene electrochemical reaction at various carbon nanomaterials like multiwalled carbon, single-walled carbon, graphite, graphene oxide, and carbon nanofiber revealed that graphitic structure (without any oxygen functional groups) and its π – π bonding are key factors for the success of the electrochemical reaction. The coronene molecular redox peak showed an unusual electrocatalytic reduction of hydrogen peroxide similar to the peroxidase enzyme-biocatalyzed reduction reaction in physiological solution.



1. INTRODUCTION

Tuning the electrochemical property of carbon nanomaterial by structure–activity relationship is a cutting-edge research in material science. Graphene, a wonderful two-dimensional (2D) material, with a honeycomb lattice-like sp^2 carbon structure differing distinctly from that of other carbon allotropes like diamond, has emerged as an advanced carbon nanomaterial for electronic devices, biomedical, conducting materials, and mechanical systems owing to its extraordinary physical properties like high surface area, thermal and electrical conductivity, and mechanical strength.^{1–3} Electron-transfer (ET) reaction is one of the important physical properties that have been achieved in graphene after functionalized with oxygen,^{4–6} metal,^{7–11} metal complex,^{12–15} and redox-active

organic species.^{16–18} Although there has been a significant number of reports on the electrochemical activity of graphene and its related materials,^{19–21} the pristine-graphitized mesoporous carbon material (GMC) is never reported for any redox activity. Herein, we observe an intrinsic electron-transfer activity of a graphene molecular model, coronene (Cor),

Received: March 21, 2020

Accepted: April 27, 2020

Published: May 11, 2020



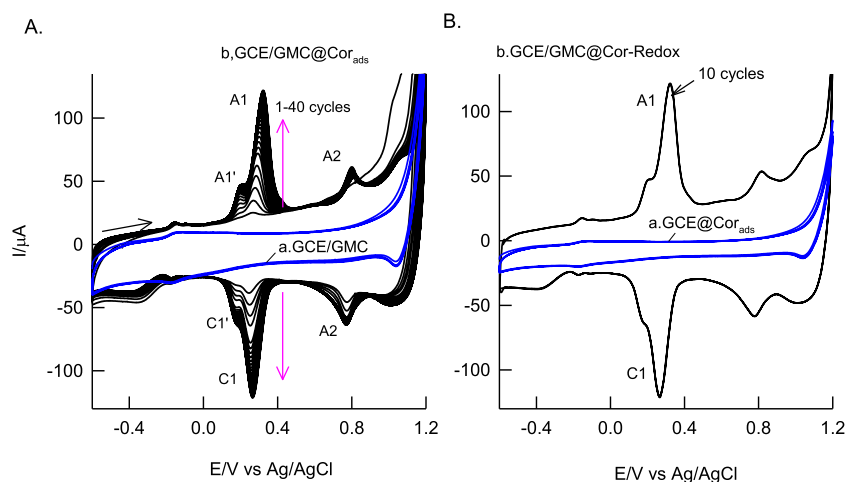


Figure 1. (A) Forty continuous CV responses of GCE/GMC (a) and GCE/GMC@Cor_{ads} (b), where ads = adsorbed in pH 2 KCl–HCl at $\nu = 50$ mV s⁻¹. (B) Twenty continuous CV responses of GCE@Cor_{ads} (a) and GCE/GMC@Cor-Redox (b) in pH 2 KCl–HCl solution.

after being π -self-assembled on graphitic materials like graphite, multiwalled carbon nanotube (MWCNT), single-walled carbon nanotube (SWCNT), and graphitized mesoporous carbon material (GMC). A specific and highly symmetrical surface-confined redox peak (Cor-Redox) at an apparent standard electrode potential $E^{\circ'} = 0.235$ V vs Ag/AgCl was noted.

Coronene, a unique polyaromatic hydrocarbon molecule (PAH) that has a central ring shared with six adjacent rings, is known as a superbenzene molecule that occurs naturally in sedimentary rock and also found in the petroleum refining process of hydrocracking.^{22,23} Its sp² carbon structure has shown a major interest in preparing several π -conjugated organic materials^{24,25} and further electronic²⁶ and optoelectronic devices,²⁴ Li-ion batteries,²⁷ and electroluminescent applications.²⁸ Owing to its complete planarity and symmetric graphitic structure (D_{6h} symmetry), it has been referred to as a model system for experimental and theoretical studies of graphene. For instance, hydrogen adsorption,²⁹ hydrogenation,³⁰ anion $\cdots\pi$ interactions in oxoanion–graphene complex,³¹ and electronic properties³² have been studied using coronene as a model system for graphene. Indeed, electrochemical studies of coronene were rarely reported in the literature. In 1996, Jia et al. first observed the redox activity of coronene derivative, tetrathiafulvalene (TTF)-fused coronene, due to one electron transfer of its radical species at $E^{\circ'} = 0.6$ V vs ferrocene/ferrocenium ion in organic medium on the Pt electrode surface.³³ In 1996, Yoshida et al. reported a coronene cationic species GaCl₂ crystalline salt, (coronene)₅(GaCl₄)₂, prepared by the galvanostatic electrochemical oxidation of coronene in the presence of GaCl₄⁻ anion, in dichloromethane/methanol mixed solution.³⁴ A crystallographic investigation of the (coronene)₅(GaCl₄)₂ salt reveals the existence of π -stacking columns of coronene cationic species in a zigzag manner in that molecular system.³⁴ In line with this context, in 2014 and 2019, Yoshida et al. prepared (coronene)₃Mo₆Cl₁₄ and (coronene^{•+})(FeBr₄⁻) salts and demonstrated the three-dimensional (3D) molecular conducting behavior (electron hopping process) of the cationic radical species.^{35,36} The background and origin of those research works is alkali-metal-ion (A)-doped fullerene, A₃C₆₀, which exhibit a π -conjugated network structure of the C₆₀ radical anion moiety.³⁷ Interestingly, first time in this work, a unique redox property

of coronene molecule, due to the existence of coronene cation radical species, after being π -self-assembled on carbon nanomaterial-modified glassy carbon electrode and performed an electrochemical oxidation reaction at 1.2 V vs Ag/AgCl in pH 2 KCl–HCl solution, was demonstrated. The redox peak was found to be highly symmetrical (tested by the cyclic voltammetry technique) and showed enzyme-free reduction of hydrogen peroxide in neutral pH solution. The aim and objective of this work are to explore the unique redox activity of the coronene self-assembled carbon nanomaterial for electrochemical application.

2. RESULTS AND DISCUSSION

2.1. Electrochemical Behavior of Coronene on Carbon Nanomaterial. Initial experiments were carried out using GMC as a base material since it has attractive physical properties like graphitic units, high surface area, mesoporous structure, and favorable holding of macromolecules like coronene. Curve a in both Figure 1A,B shows 10 continuous CV responses of coronene-adsorbed glassy carbon electrode, GCE/Cor_{ads}, and unmodified GCE/GMC, respectively, in pH 2 KCl–HCl solution. As can be seen, there is no faradic electron-transfer activity on the modified systems indicating the nonamenable electrochemical characteristic of coronene molecule and GMC, respectively, under independent condition. The superaromatic activity (nonconducting) with rigid molecular network structure is a likely reason for the failure (coronene). Interestingly, when the coronene molecule was adsorbed on GCE/GMC, i.e., GCE/GMC@Cor_{ads}, and performed continuous CVs in pH 2 KCl–HCl, a well-defined growth like redox current pattern at an apparent standard electrode potential $E^{\circ'} = 0.235 \pm 0.005$ V vs Ag/AgCl (A1/C1) was noted (Figure 1A, curve b). Figure 1B shows 10 continuous CV responses of the electrochemically treated GCE/GMC@Cor_{ads}, showing a stable response with a peak-to-peak potential difference ($\Delta E_p = E_{pa} - E_{pc}$, where E_{pa} and E_{pc} are anodic and cathodic peak potentials, respectively) of ~ 0 V. The calculated surface excess value is $\Gamma_{\text{Cor-Redox}} = 10.1 \times 10^{-9}$ mol cm⁻². Hereafter, the coronene chemically modified electrode is designated as GCE/GMC@Cor-Redox.

In general, redox-mediated chemically modified electrodes show a large potential difference in ΔE_p ,^{18,38,39} which may be due to inhomogeneity, finite mass and charge transport, and

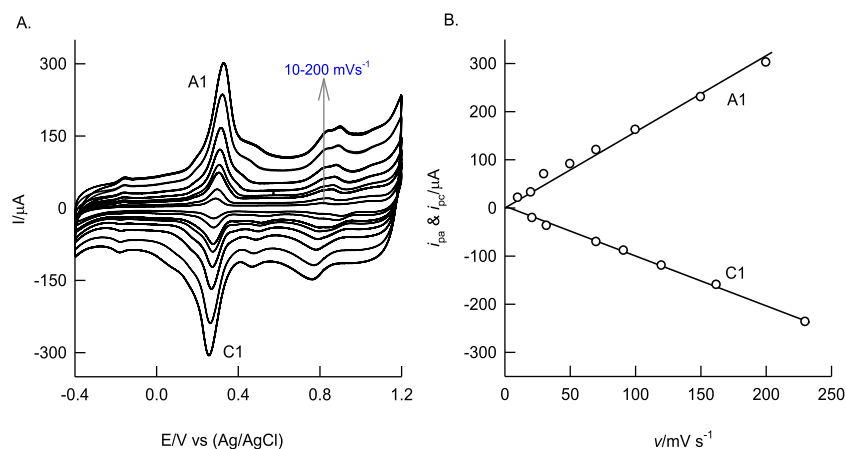


Figure 2. Effect of CV scan rate on GCE/GMC@Core-Redox in pH 2 HCl/KCl (A) and its i_{pa} and i_{pc} vs scan rate plot (B).

structural and resistive changes in the film.³⁹ On the other hand, a perfect bell-like redox peak response with $\Delta E_p \sim 0$ V noted in this work attributes a strong adsorption and minimum resistive change of the electroactive coronene molecule on the chemically modified electrode.

The effect of scan rate showed a regular increase in the anodic and cathodic peak currents against an increase in the scan rate (Figure 2A). The plot of i_{pa} and i_{pc} vs ν is found to be linear starting from the origin point, due to the surface-confined electron-transfer activity of the coronene redox peak (Figure 2B). Figure 3A shows the effect of solution pH on the

CV response of the modified electrode. A plot of $E^{o'}$ vs pH showed a linear line with a negative slope, -56 ± 2 $mV pH^{-1}$ due to the proton-coupled electron-transfer activity of the redox peak with the involvement of the Nernstian type of $E-pH$ behavior, i.e., -60 $mV pH^{-1}$. Based on literature reports,^{33–36} the key site of electroactive coronene generated on the modified electrode is proposed as a cationic radical species. At this stage, it is difficult to predict the molecular structure of the coronene cationic radical species using a spectroscopic technique like GC-MS, due to the instability of the intermediate species without the carbon matrix. Moreover, since the amount of Cor-Redox species formed on the surface is about the nanogram level, it is difficult to perform a nuclear magnetic resonance (NMR)-based characterization study that requires sample about the milligram level. To solve this problem and to find out the true active redox species of the coronene, several critically designed control experiments and physicochemical characterizations of the chemically modified electrode were performed.

Figure 4A shows the CV responses of GCE/GMC@Cor_{ads} at different potential windows. Freshly prepared electrodes were used for this purpose. Experiments were performed to understand the effect of applied potential on the preparation of GMC@Cor-Redox system. In this CV experiment, the starting cathodic potential was fixed at -0.2 V and the anodic potential was varied as 1.2 V (a), 1.0 V (b), 0.9 V (c), 0.8 V (d), 0.7 V (e), and 0.6 V vs Ag/AgCl (f). It is obvious to see an emergence of A1/C1 redox peak, only when the anodic potential is swept to 1.2 V vs Ag/AgCl (curve a). To substantiate the observation, discrete potentiostatic polarization experiments at various sets of applied potentials (E_{app}) from 0.6 to 1.2 V vs Ag/AgCl were carried out with GCE/GMC@Cor_{ads}. Figure 4B is a plot of i_{pa} (A1 peak) vs E_{app} , wherein ~ 100 times higher A1 peak current value, when E_{app} is set at 1.2 V vs Ag/AgCl, over the current response measured at $E_{app} = 0.8$ V, was noted. This observation attributes a specific role of the high anodic potential, 1.2 V, vs Ag/AgCl on the surface-bound oxidation of coronene on GMC. Note that at a high applied potential, 1.2 V vs Ag/AgCl, the oxidation of water to dioxygen via hydroxy radical formation reaction is significant.^{40,41} It is likely that at a high oxidation potential, hydroxyl radical-like intermediate species are formed on the interface⁴¹ and assisted the oxidation of the surface-confined coronene molecule to coronene radical species (A1/C1 redox peak). This observation is correlated with the literature reports

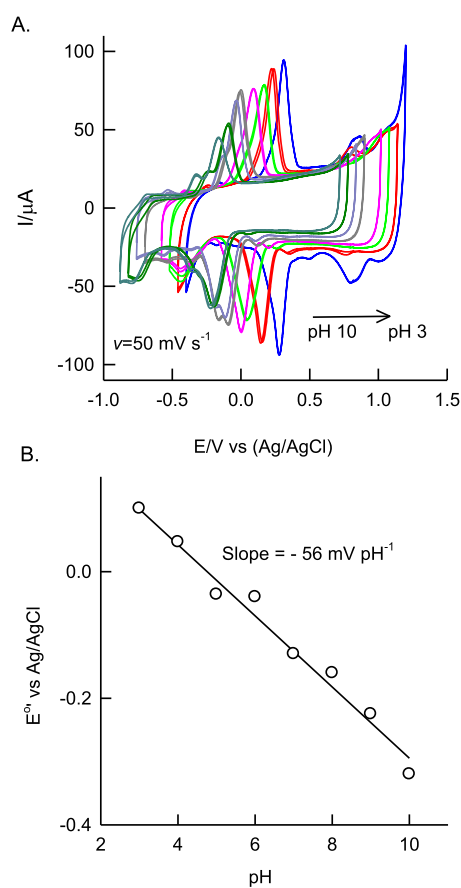


Figure 3. Effect of solution pH on the CV response (two cycles) of GCE/GMC@Cor-Redox at $\nu = 50$ $mV s^{-1}$ (A). Plot of $E^{o'}$ vs pH (B).

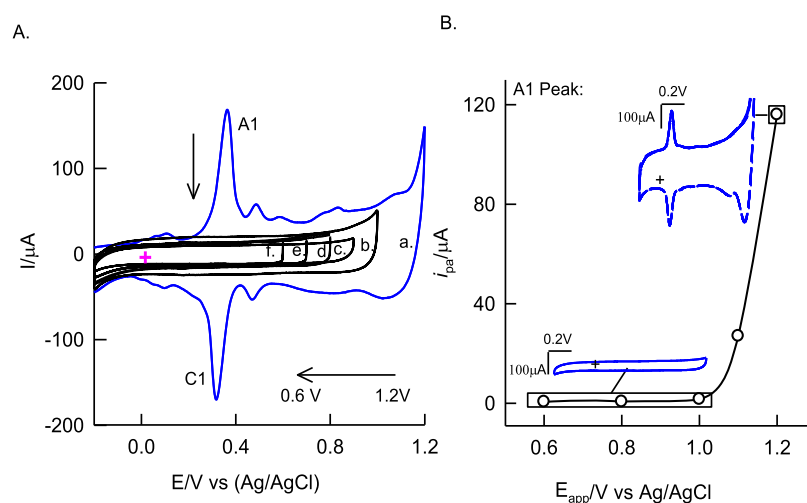


Figure 4. Effect of potential scan direction on the CV response of GCE/GMC@Cor_{ads} in pH 2 HCl/KCl at $\nu = 50 \text{ mV s}^{-1}$. Fresh prepared electrodes were used for each scan. (A) E-cycling experiments with a fixed cathodic potential, -0.2 V , and varying anodic potentials: (a) 1.2 V , (b) 1.0 V , (c) 0.9 V , (d) 0.8 V , (e) 0.7 V , and (f) 0.6 V vs Ag/AgCl. (B) Effect of applied potential (E_{app}) on the potentiostatic preparation of GCE/MWCNT@Cor-Redox in pH 2 HCl/KCl.

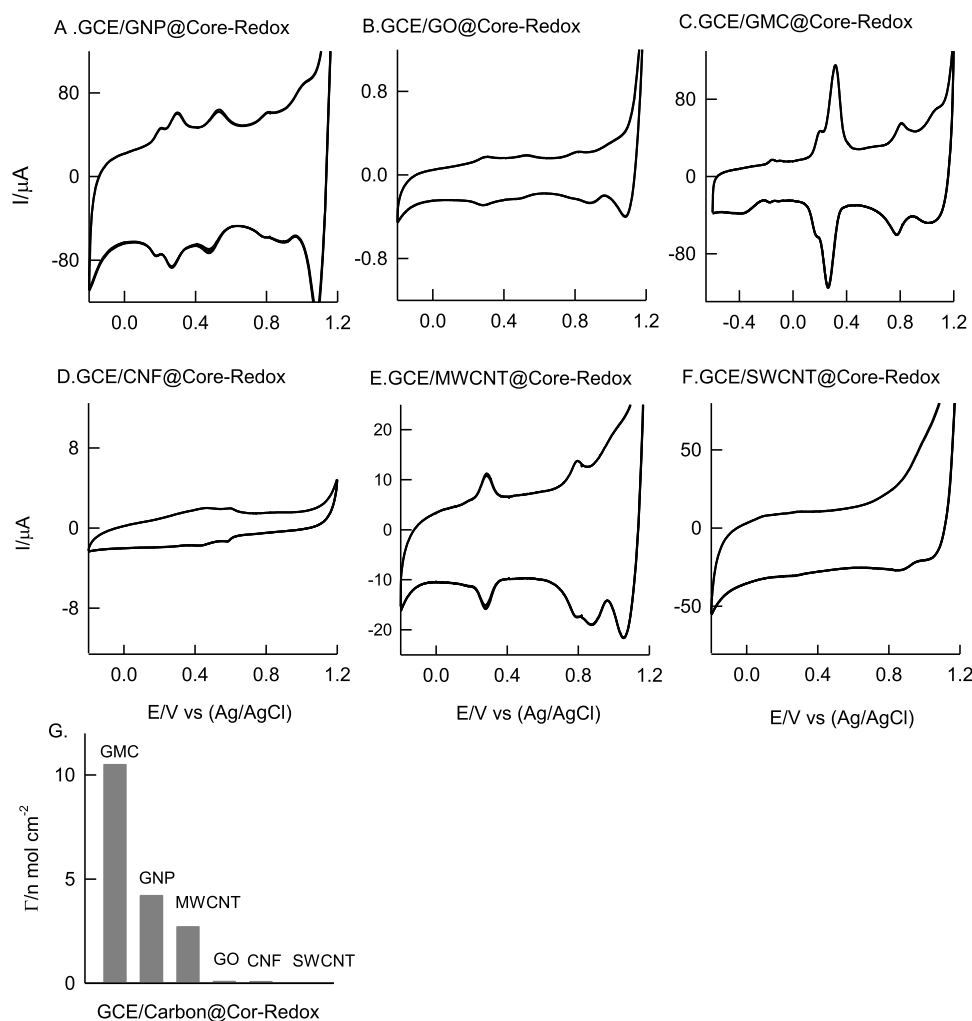


Figure 5. (A–F) CV responses of various carbon nanomaterials surface-confined Cor-Redox-modified GCEs in pH 2 HCl/KCl at a scan rate of 50 mV s^{-1} . (G) Plot of $\Gamma_{\text{Cor-Redox}}/n$ vs GCE/Carbon@Core-Redox. GNP = graphite nanopowder; GO = graphene oxide; GMC = graphitized mesoporous carbon; CNF = carbon nanofiber; MWCNT = multiwalled carbon nanotube; and SWCNT = single-walled carbon nanotube.

of reactive oxygen species (ROS)-assisted one-electron oxidation of polyaromatic hydrocarbon to respective cation

radical species.^{42,43} Based on this information, it is proposed that the coronene molecule oxidized to coronene cationic

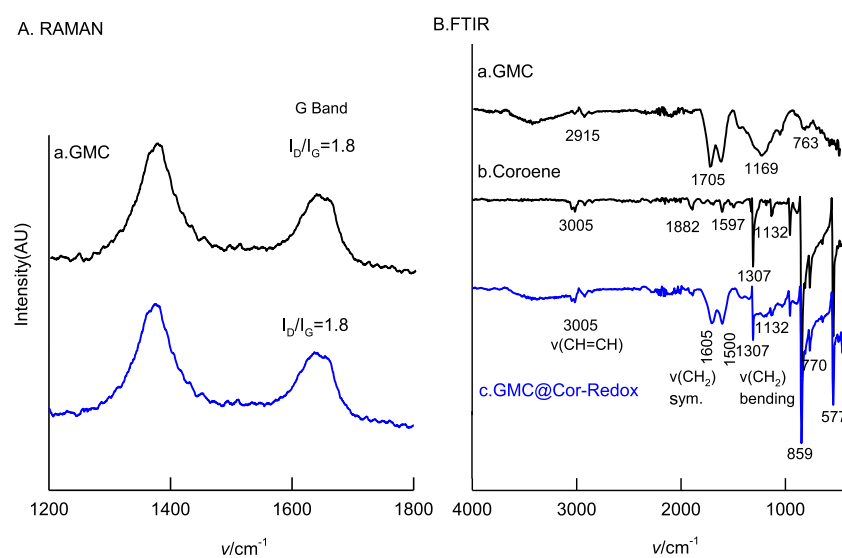


Figure 6. Comparative (A) Raman and (B) FTIR spectroscopic responses of GMC@Cor-Redox sample along with other controls.

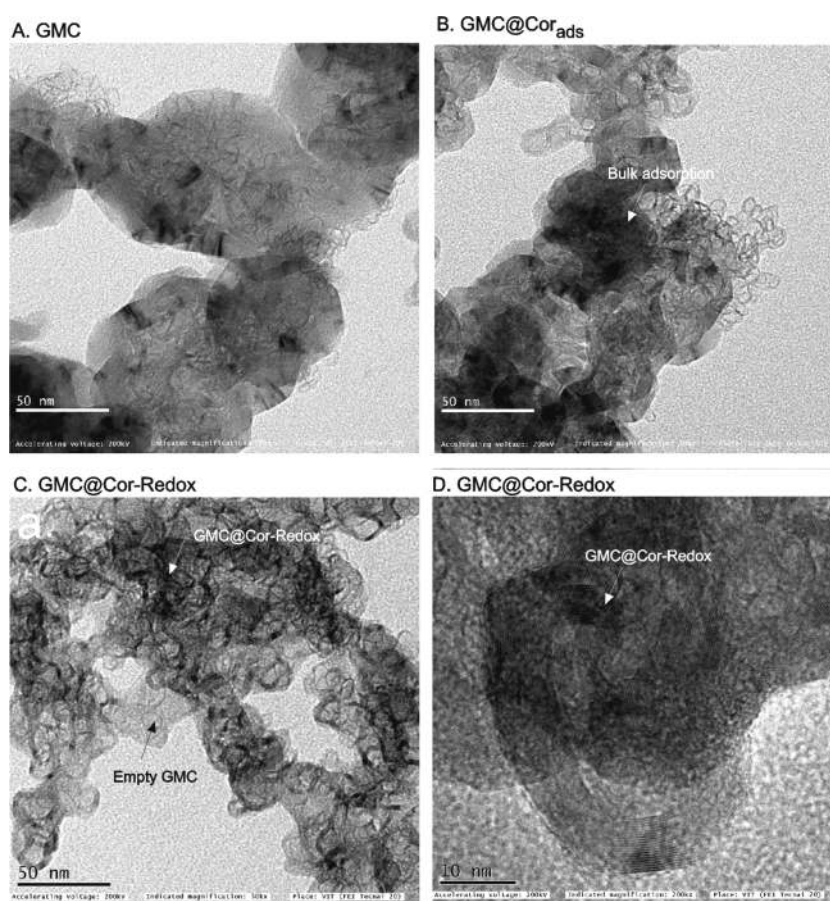


Figure 7. TEM images of GMC (A), GMC@Cor_{ads} (before CV experiment) (B), and GMC@Cor-Redox at different magnifications (C, D). Cor_{ads} = coronene adsorbed.

radical intermediate species (Coronene^{•+}) on the surface of carbon nanomaterial and showed a redox peak at $E^{\circ'} = 0.235$ V (A1/C1). The additional peaks noted at $E^{\circ'} = 0.2$ V (A1'/C1') and 0.7 V vs Ag/AgCl (A2/C2) are proposed as redox responses of coronene at energetically different carbon sites. A similar kind of multiple peak observation was noted when anthraquinone is adsorbed on the MWCNT-modified GCE electrode.⁴⁴

With the aim to understand the effect of carbon surface functionalities like graphitic unit, oxygen functional group, and porous structure, various carbon materials like graphite nanopowder (GNP), graphene oxide (GO), carbon nanofiber (CNF), multiwalled carbon nanotube (MWCNT), and single-walled carbon nanotube (SWCNT) were subjected to coronene electrochemical oxidation reaction and the respective GCE/carbon@Cor-Redox chemically modified electrode for-

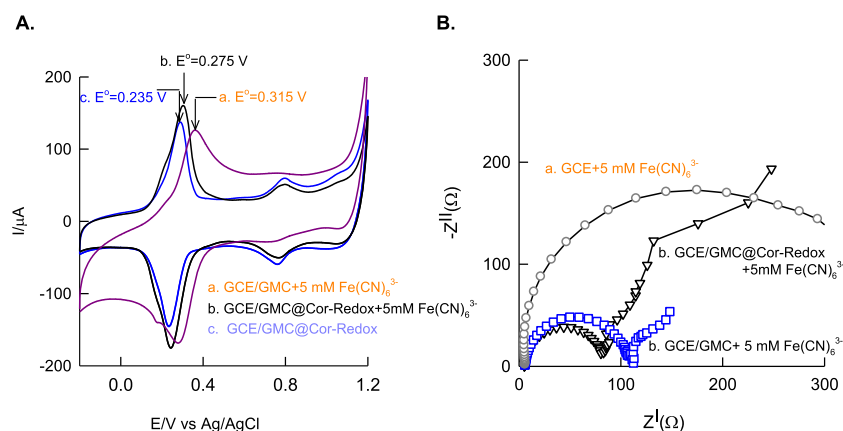


Figure 8. Comparative CV (A) responses of GCE@GMC (a) and GCE/GMC@Cor-Redox without (c) and with 5 mM $\text{Fe}(\text{CN})_6^{3-}$ (b) in pH 2 HCl/KCl at 10 mV s^{-1} vs Ag/AgCl. (B) Comparative EIS responses of GCE (a), GCE/GMC@Cor-Redox (b), and GCE@GMC (c) with 5 mM $\text{Fe}(\text{CN})_6^{3-}$ in pH 2 HCl/KCl at a biased potential. 0.25 V vs Ag/AgCl.

mation. As can be seen in Figure 5, except CNF and SWCNT cases, other carbon matrices showed qualitatively similar voltammetric responses. Based on the surface excess value ($\Gamma_{\text{Cor-Redox}}$), the order of carbon for the Cor-Redox peak formation was sequenced as follows: GMC ($10.1 \times 10^{-9} \text{ mol cm}^{-2}$) > GNP ($4.2 \times 10^{-9} \text{ mol cm}^{-2}$) > MWCNT ($2.7 \times 10^{-9} \text{ mol cm}^{-2}$) > GO ($0.08 \times 10^{-9} \text{ mol cm}^{-2}$) > CNF ($0.07 \times 10^{-9} \text{ mol cm}^{-2}$) > SWCNT ($0.001 \times 10^{-9} \text{ mol cm}^{-2}$). From the collective information obtained from experimental observations, the following conclusions were made: (i) multilayer graphitic structure is necessary for the coronene electrochemical oxidation reaction. Presumably, there is a strong π - π interaction between the graphite structure and aromatic carbons of coronene, i.e., diffusion-restricted electrochemical oxidation reaction. (ii) Carbon-oxygen functional groups such as hydroxyl, carboxylic acid, phenolic, alcoholic, and ether are not favorable for the Cor-Redox formation. It is likely that the oxygen functional groups quench the coronene cationic radical species, thereby reducing the redox activity. (iii) The porous structure of GMC helped in rich surface confinement of the Cor-Redox system in addition to the π - π interaction. Since the GMC material showed the best response for Cor-Redox behavior, it has been chosen as a model system for further investigation.

2.2. Physicochemical Characterizations. Figure 6A shows a comparative Raman spectroscopic response of GMC and GMC@Cor-Redox. Unmodified GMC showed Raman signals at 1350 and 1550 cm^{-1} corresponding to the disordered (D, sp^3 carbon network) and ordered graphitic (G, sp^2 carbon network) structures of the carbon material. The calculated intensity ratio, $I_{\text{D}}/I_{\text{G}} = 1.8$, indicates an appreciable graphitic network structure with the GMC. After the Cor-Redox modification, the intensity of the D band signal is found to be unaltered ($I_{\text{D}}/I_{\text{G}} = 1.8$). This observation reveals the retention of the graphitic structure of the GMC@Core-Redox and GMC systems. Initially, it was thought that coronene is oxidized to coronene-quinone like a molecule similar to our previous work on the oxidation of anthracene to anthraquinone on the MWCNT surface,⁴⁵ which shows a marked improvement in the D signal due to the conversion of sp^2 to sp^3 carbon formation.⁴⁶ The Raman spectroscopic result of unalteration in the graphitic structure rolled out the possibility of the coronene-quinone like molecular formation in this work. Further, to probe the molecular structure details, FTIR

spectroscopy of GMC@Cor-Redox was carried out in comparison to GMC and coronene as control samples. Specific IR signals for hydroxyl functional group (3500 cm^{-1}) and $\text{CH}=\text{CH}_2$ (3005 , 1605 , 1500 , and 1307 cm^{-1}) sites with GMC and $-\text{CH}=\text{CH}_2$ functional group (3005 , 1882 , 1597 , 1132 , and 859 cm^{-1}) with coronene molecule were noted (Figure 6B).⁴⁷ Interestingly, the IR spectra of GMC@Cor-Redox showed signals corresponding to the individuals of both GMC and coronene molecules without any new and addition peak formation. This observation confirms the existence of a native-like form of the coronene molecule, i.e., coronene cation radical species, without any quinone functional group formation (peak at ca. 1650 – 1750 cm^{-1}). Figure 7A–D shows comparative transmission electron microscopy (TEM) images of pristine GMC, GMC@Cor_{ads} (before CV experiment), and GMC@Cor-Redox (after the experiment) at different magnifications. The GMC@Cor_{ads} sample showed bulk dark spots like an image, whereas GMC@Cor-Redox (after CV experiment) showed the dark spots concentrated on the fine edges of the GMC. The dark spots noted are the sites of the Cor-Redox molecules that have been π -self-assembled on the graphitic base of the GMC. It is obvious to see the fringes of the graphitization layer even after the Cor-Redox modification supporting the π -self-assembly and stacking of the Cor-Redox on the graphitic underlying structure.

2.3. Electrochemical Characterization. The electronic property of the GMC@Core-Redox system was tested by subjecting it with a standard redox couple in homogeneous condition as a model system. In the literature, the ferricyanide/ferrocyanide redox couple has been widely used as a tool, wherein the dependence of the electronic structure and conductivity and the alteration in the redox peak current were noted.^{47,48} Since i_{pa} or $i_{\text{pc}} \propto$ electrochemical accessible surface area, according to the Randles-Sevcik equation,³⁹ if Cor-Redox has electronic property, then a significant increment in the redox current response and decrement in ΔE_{p} will be noted. On the other hand, the absence of any such alteration in the current and ΔE_{p} response can be referred to as the absence of electronic property of the modified electrode. Note that coronene is an example of the insulator type of organic molecule. Figure 8A shows a comparative CV response of GCE/GMC@Cor-Redox and GCE/GMC with 5 mM $\text{Fe}(\text{CN})_6^{3-}$ in pH 2 KCl–HCl solution. A well-defined redox peak for the reversible electron-transfer feature of

$\text{Fe}^{\text{III}}(\text{CN})_6^{3-/4-}$ was obtained. Indeed, due to the closer $E^{\circ'}$ potentials, both Cor-Redox ($E^{\circ'} = 0.235$ V vs Ag/AgCl) and $\text{Fe}(\text{CN})_6^{3-}$ ($E^{\circ} = 0.315$ V vs Ag/AgCl) signals overlapped and showed a single redox signal at $E^{\circ} = 0.275$ V vs Ag/AgCl. Note that the obtained $E^{\circ'}$ value of the ferricyanide/ferrocyanide redox couple on GCE/GMC@Cor-Redox (0.275 V) is in between the values of GCE/GMC@Cor-Redox (0.235 V) and GCE/GMC + ferricyanide ($E^{\circ} = 0.25$ V). In addition, GCE/GMC@Cor-Redox showed about 10% increment in the peak current compared to other peak current signals (Figure 8A). This observation reveals a mixed-potential mechanism of the electrochemical reaction,⁴⁹ wherein the individual electron-transfer systems Cor-Redox and $\text{Fe}(\text{CN})_6^{3-}$ interacted with each other. The mixed-potential mechanism is a common phenomenon in corrosion reactions.^{50,51}

Figure 8B shows electrochemical impedance spectroscopic responses of GCE/GMC@Cor-Redox and GCE/GMC with a 5 mM $\text{Fe}(\text{CN})_6^{3-}$ system at pH 2 KCl–HCl. Defined semicircles, which are due to the charge-transfer (R_{CT}) characteristic of the systems, were noted. Based on the Randles circuit, calculated R_{CT} values for ferricyanide oxidation at GCE, GCE/GMC, and GCE/GMC@Cor-Redox are 1611, 161.3, and 135.8 Ω , respectively. The observation of the lowest R_{CT} value (135.8 Ω) with GCE/GMC@Cor-Redox compared to other systems indicates enhanced electronic and surface properties of GCE/GMC@Cor-Redox.⁵² The existence of coronene radical cationic species is the reason for the observation. To substantiate the result, a radical scavenger, (2,2,6,6-tetramethylpiperidin-1-yl)oxyl, TEMPO, has been examined with the GCE/GMC@Cor-Redox system. Curve a in Figure 9 shows a control CV response of GCE/GMC with

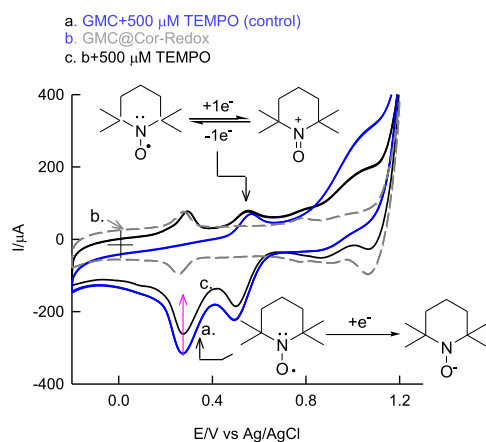


Figure 9. CV response of (a) GCE/GMC with 500 μM TEMPO and GCE/GMC@Cor-Redox without (b) and with 500 μM TEMPO (c) in N_2 purged in pH 2 HCl/KCl at $v = 50$ mV s^{-1} . The insets show the electrochemical reactions of TEMPO.

500 μM TEMPO in the N_2 -purged pH 2 KCl–HCl solution. An irreversible reaction followed by redox electron-transfer process due to the aminoxy anion/TEMPO radical (I) and TEMPO radical/oxoammonium cation (II/III) electrochemical reactions, respectively,⁵³ was noted. When the same experiment was carried out on GCE/GMC@Cor-Redox, a marked reduction in the irreversible signal due to quenching of Cor-cationic radical species by TEMPO radical was observed. Note that similarly to the ferricyanide redox system, TEMPO electron-transfer behavior is also found to overlap with the Cor-Redox process due to the mixed-potential mechanism.

These observations reveal the existence of cationic radical-redox species with the Cor-Redox system^{33–36} rather than the dielectric behavior of the natural coronene.

Figure 10 shows the typical X-ray photoelectron spectroscopy (XPS) analysis data for GMC@Cor-Redox in comparison to the GMC@Cor_{ads} system. Core energy levels C 1s and O 1s were considered for the comparison. A marked signal at binding energy (BE) = 284.6 eV, which is due to sp^2 and sp^3 carbons of GMC, was noted. In addition, minor fractions due to carbonyl ($>\text{C}=\text{O}$) and alcohol/phenol ($-\text{C}-\text{OH}/\text{Ph}-\text{OH}$) at BE = 285.4 and 287.4 eV, respectively, were also noted.⁵⁴ This observation was reflected in characteristic BE values of O 1s core energy at 531.3 and 532.4 eV, respectively (1).⁵⁵ XPS characterization data of the electrochemically oxidized GMC@Cor_{ads}, i.e., GMC@Cor-Redox, showed a unique pattern (Figure 10b). It was found that the C 1s signals remained constant (data in parallel with Raman spectroscopic results), whereas the O 1s signal increased markedly at BE = 532.9 eV. A similar kind of observation was reported previously by Herrmann-Geppert et al. for the plasma-treated $\alpha\text{-Fe}_2\text{O}_3$ (hematite) film for the oxygen gas evolution reaction and it has been revealed that new oxygen species like oxy hydroxyl radical-like OH species are formed/trapped on the surface.⁵⁶ Presumably, at a high applied potential of preparation, 1.2 V vs Ag/AgCl (Figures 1 and 4), water molecules oxidized as the oxygen molecule via oxy and hydroxyl radical intermediates and further involved in the electrochemical oxidation of coronene to coronene-cationic radical species (Cor-Redox) on the modified electrode surface (Scheme 1C). Based on the results, the unusual O 1s species identified in the XPS analysis is correlated to the oxy/hydroxyl radical species stabilized/trapped on the GMC-modified electrode surface without affecting the graphitic network structure.

To understand the unique surface property, GCE/GMC@Cor-Redox was further explored by the scanning electrochemical microscope (SECM) technique coupled with the ferricyanide/ferrocyanide redox system in pH 2 KCl–HCl. For that, a GMC@Cor-Redox layer was formed on an SECM–Au working electrode substrate according to the procedure shown in Figure 1A. A 10 μm Pt ultramicroelectrode has been used as a Tip for the SECM measurements. A feedback mode SECM technique, wherein the tip current was obtained due to the counter reaction of substrate (Sub), was adopted (under bipotentiostatic condition) (Figure 11A). Prior to the studies, interrelated potential parameters were optimized as $E_{\text{sub}} = 0.2$ V (where $\text{Fe}^{\text{III}}(\text{CN})_6^{3-} + \text{e}^- \rightarrow \text{Fe}^{\text{II}}(\text{CN})_6^{4-}$) and $E_{\text{Tip}} = 0.4$ V vs Ag/AgCl (where $\text{Fe}^{\text{II}}(\text{CN})_6^{4-} \rightarrow \text{Fe}^{\text{III}}(\text{CN})_6^{3-} + \text{e}^-$) using the approach curve method. Figure 11A,B shows the comparative SECM morphology images of the Au/GMC@Cox-Redox and Au/GMC (control) systems. A flat surface-active layer-like response with an enhanced current signal, which may be due to the surface cationic/oxygen radical species, was noted with the GCE/GMC@Cox-Redox system. It is likely that since the Cor-Redox is immobilized on GMC via strong multilayer π – π interactions uniformly, there is no specific signal for the pores and redox sites of GMC@Cor-Redox. This qualitative information supports the enhanced electronic function of GMC@Cor-Redox.

2.3.1. Electrocatalytic Reduction of Hydrogen Peroxide. In addition to electrochemical characterization, GCE/GMC@Cor-Redox is subjected to redox probe-sensitive electrocatalysis experiment in pH 7 phosphate-buffered saline (Figure 12A). Previously, our group used the redox probe character-

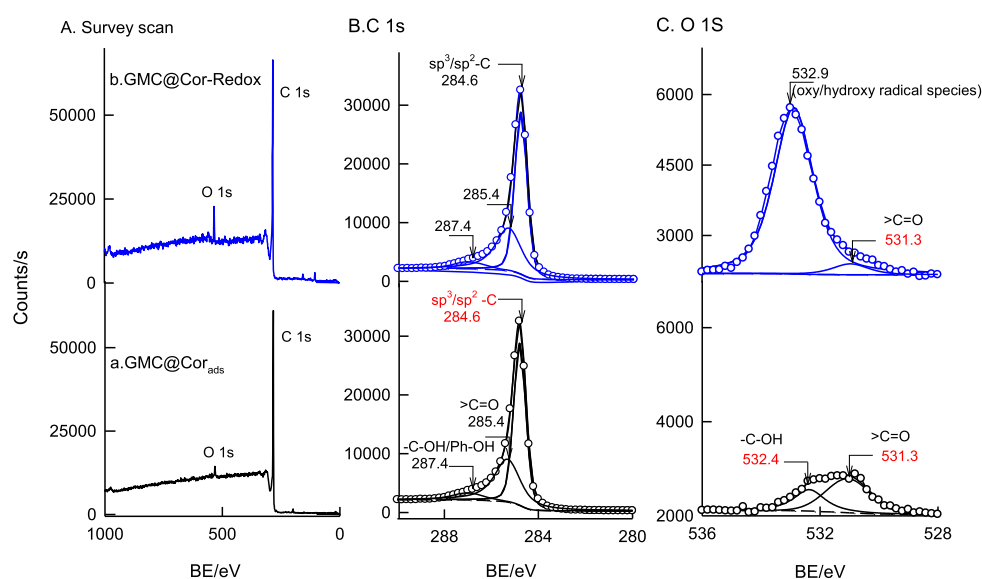
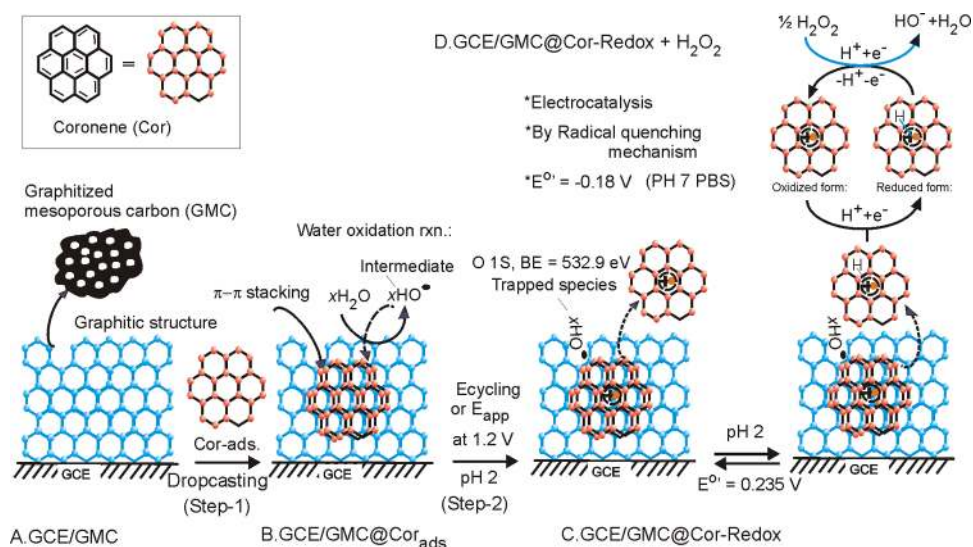


Figure 10. XPS characterization data of SPE/GMC@Cor_{ads} (a) and SPE/GMC@Cor-Redox (b) systems. (A) Survey scan, (B) C 1s, and (C) O 1s energy-level diagrams.

Scheme 1. Cartoons Illustrating (A) GMC and Graphene Subunit, Coronene (Cor); (B) Physisorption of Cor as π -Stacking on Graphitic Surface of GMC-Modified GCE, GCE/GMC@Cor_{ads}; (C) Electrochemical Reaction-Assisted Oxidation of the Surface-Confining Coronene, GCE/GMC@Cor_{ads} to Redox-Active Compound, GCE/GMC@Cor-Redox via Hydroxyl Radical Species Formed on Oxygen Evolution Reaction; and (D) Electrocatalytic Reduction of H₂O₂ by the GCE/GMC@Cor-Redox in pH 7 Phosphate-Buffered Saline



ization technique to identify some of the specific oxidation states of ruthenium, (VI/IV) and (VII/IV), using formaldehyde and glucose oxidation reactions, respectively.⁵⁷ In this work, to verify the existence of redox-active 1,2-dihydroxy and 1,4-dihydroxy benzene derivatives of coronene, a selective organic probe, cystein, was subjected to electrochemical study.³⁸ Note that 1,2-dihydroxy and 1,4-dihydroxy benzene derivatives involved in the proton-coupled electron-transfer reaction for the formation of respective quinone, which can mediate the chemical oxidation of cysteine molecules. The absence of CySH electrocatalysis can be indirectly considered as evidence for the absence of any dihydroxy benzene functional group. The CV response of the GCE/GMC@Cor-Redox system with and without 1 mM CySH showed nil peak current increment confirming the absence of any hydroxyl

functional group with the Cor-Redox system (Figure 12B). On the other hand, GCE/GMC@Cor-Redox showed a profound mediated reduction signal to hydrogen peroxide without any dissolved oxygen interference (Figure 12C). The mechanism proposed here is due to the coronene cationic radical-mediated reaction, as displayed in Scheme 1D and the inset of Figure 12C. It is noteworthy that organic redox molecules have been rarely reported for the mediated reduction of hydrogen peroxide without the support of protein such as cytochrome c, peroxidase, and hemoglobin in a neutral solution.⁵⁸ Indeed, metal and its derived compounds are proven for the H₂O₂ interaction.⁵⁹ The specific electrocatalytic observation demonstrated in this work not only evidences the radical quenching reaction similar to TEMPO but also the high significance of biomimicking electrocatalytic reduction and sensing of H₂O₂

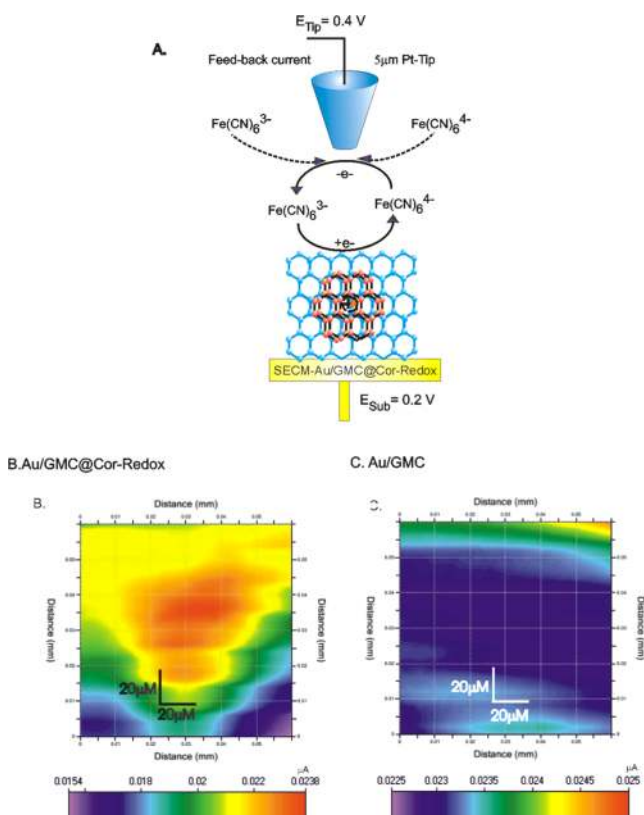


Figure 11. Scanning electrochemical microscope results. (A) Cartoon of the feedback current signal from the SECM experiment. Typical SECM hotspot images of (B) Au/GMC@Cor-Redox and (C) Au/GMC (control) by 10 μm Pt tip, when the substrate is conditioned at 0.2 V vs Ag/AgCl and $E_{\text{Tip}} = 0.4$ V vs Ag/AgCl in pH 2 KCl–HCl solution.

in physiological condition. Overall, the Cor-Redox peak observed in this work is a novel observation in material science and has beneficial effects in a variety of electrochemical fields.

3. CONCLUSIONS

Electrochemical oxidation of coronene on graphitic mesoporous carbon (GMC)-modified glassy carbon electrode showed the emergence of a unique redox peak at $E^{o'}$

0.235 V vs Ag/AgCl in a pH 2 KCl–HCl solution. The redox peak is found to be adsorption-controlled and proton-coupled electron transfer in nature. It is important to note that a highly symmetrical behavior of the redox peak, wherein the peak-to-peak potential separation is nearly 0 V, due to the efficient self-assembly of the redox-active coronene molecule on the graphitic structure of GMC, was noted. The effect of potential window on the electrochemical oxidation of GCE/GMC@Coronene_{ads} showed the specific influence of the high applied potential, 1.2 V, vs Ag/AgCl on the oxidation of the coronene. The investigation of Cor-Redox peak formation on various carbon materials indicated that the existence of graphitic layer without any oxygen surface functional is a favorable condition for a successful preparation. Based on the experimental observation and literature reports, it has been proposed that upon high-potential oxidation (1.2 V), the water molecule gets oxidized to dioxygen along with hydroxyl radical intermediate species that oxidize the surface-confined coronene as a coronene cationic radical species. The following evidences were provided in this manuscript for the radical species: (i) appearance of a redox peak of the coronene, (ii) radical quenching species, TEMPO interaction on this new system, (iii) a new XPS characterization support for the appearance of radical-like species on the surface, and (iv) electrochemical-mediated reduction of OH radical from H_2O_2 by coronene cationic radical species. The existence of a strong π – π interaction between the graphitic structure of GMC and aromatic π -electrons of coronene and its diffusion-restricted oxidation reaction are the key steps for the success of the oxidation reaction. The GMC@Cor-Redox system was subjected to Raman, IR, XPS, TEM, and control electrochemical characterization studies including scanning electrochemical microscope imaging with ferricyanide as a redox probe and electron-scavenging redox probe, TEMPO. Collective information from the experiments confirmed that Cor-Redox is π -self-assembled on the graphitic structure of GMC and cationic radical species is an electroactive site for the redox reaction. This is the first study on the selective electrocatalytic reduction of hydrogen peroxide by redox-active organic molecule, where Cor-Redox in physiological solution has been demonstrated with results comparable to those of peroxidase enzyme biocatalytic reaction. Overall, coronene cationic radical species-based symmetrical redox system and its bioelectrocatalytic reduction of H_2O_2 are new

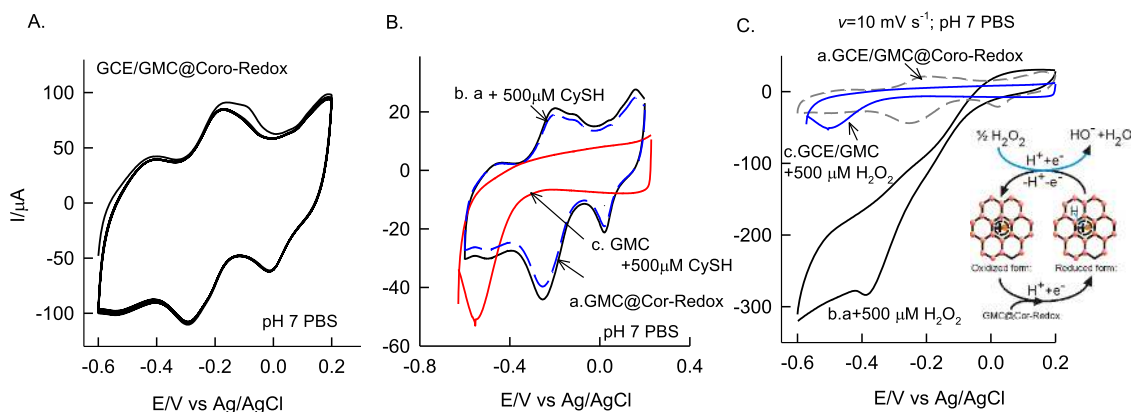


Figure 12. CV responses of (A) GCE/GMC@Coro-Redox at $v = 50$ mV s^{-1} and GCE/GMC@Coro-Redox at $v = 10$ mV s^{-1} with (b) and without 500 μM CySH (a). (B) CySH and (C) H_2O_2 in pH 7 phosphate-buffered saline (PBS). Curve c shows control CV responses of GCE/GMC with respective analytes. The inset in (C) is a cartoon for the Cor-Redox cation radical quenching-based electrocatalytic reduction of H_2O_2 .

observations in this work. Note that the coronene oxidation reaction was studied as a model electrochemical reaction on carbon material surface. We have to carry out bulk synthesis of the electrochemical reaction.

4. EXPERIMENTAL SECTION

4.1. Reagents. Coronene (97% purity), MWCNT (> 90% carbon basis, outer diameter: 10–15 nm; inner diameter: 2–6 nm; length 0.1–10 μm), single-walled carbon nanotube (SWCNT; 60–70% pure-on carbon basis, 0.7–1.1 nm diameter, 5.2 wt % metal impurities (Co, Fe, Ni)), graphitized mesoporous carbon (GMC; 99.95% purity, ~ 50 nm pore size, >200 m^2 g^{-1} surface area), graphitized carbon nanofiber (CNF; 99.9 wt %—on the carbon basis, 100 nm \times 20–200 μm), and graphite nanopowder (GNP; 400 nm size, 98% purity) were purchased from Sigma-Aldrich. Screen-printed carbon electrodes (0.3 mm diameter) were obtained as a gift from Prof Jyh-Myng Zen, Taiwan. Unless otherwise stated, 0.1 M pH 2 KCl–HCl (for preparation) and pH 7 phosphate-buffered saline (PBS, for electroanalytical application) have been used as supporting electrolytes.

4.2. Instrumentation. Electrochemical measurements were all carried out using a CHI760D electrochemical workstation. A three-electrode system consisted of glassy carbon electrode (GCE) as the working electrode (0.0707 cm^2), Ag/AgCl as the reference electrode, and Pt wire as the auxiliary electrode was used. The Bioanalytical Systems (BAS) Polishing Kit was used to polish the GCE surface. A JASCO 4100 spectrophotometer instrument was used for the FTIR analysis (by the KBr method). A HORIBA XploRA instrument, France, was used for the Raman spectroscopic analysis of the modified electrodes at a fixed wavelength of 532 nm. A PHI VersaProbe II instrument was used for the X-ray photoelectron spectroscopy analysis. For internal XPS data calibration, a binding energy (BE) of 284.6 eV was used. XPS peak fitting software was adopted for the deconvolution of the XPS data. For scanning electrochemical microscopy (SECM) studies, Princeton Applied Research, VersaSCAN Instrument, coupled with a 0.196 cm^2 Au substrate (5 mm diameter) and a 5 μm Pt tip under a bipotentiostat condition, was used. The position of the Pt tip against the SECM–Au substrate was fixed from an approach curve in the feedback mode, obtained by moving the Pt tip position at a speed of 1 μm s^{-1} in the z axis direction at a potential of 0.5 V vs Ag/AgCl, wherein the diffusion-controlled redox reaction occurred (ferricyanide + $\text{e}^- \rightarrow$ ferrocyanide). The surface concentration, $\Gamma_{\text{Cor-Redox}}$ of the electroactive Cor-Redox species responsible was calculated using the equation $\Gamma_{\text{Cor-Redox}} = Q/nFA_e$, where Q is the charge, obtained by integrating the anodic redox peak area by cyclic voltammetry at a slow scan rate of 10 mV s^{-1} , in pH 7 PBS; n is the number of electrons transferred (1 in the present case), and A_e is the electrode geometric area (0.0707 cm^2).

4.3. Preparation of the Coronene-Immobilized Carbon Nanomaterial-Modified Electrode. Although there is no qualitative difference in the electrochemical behavior, it is advised to recrystallize the coronene in benzene and use it for electrochemical studies. First, the surface of GCE was cleaned both mechanically and electrochemically by polishing with 0.5 μm Al_2O_3 powder, washing with double-distilled water, followed by performing 10 continuous CV experiments in the potential window of -0.2 to 1 V vs Ag/AgCl at a scan rate (ν) of 50 mV s^{-1} in pH 7 PBS. Then, the GCE/GMC-modified electrode, as an optimal system, was prepared by drop-coating

5 μL of an ethanol suspension containing 2 mg of GMC dissolved in it on a cleaned GCE surface and drying the electrode in air for 3 ± 1 min at room temperature (25 ± 2 $^\circ\text{C}$). Further, the GCE/MWCNT@Cor-Redox chemically modified electrode was prepared by following a two-step procedure (Scheme 1). Step 1: 5 μL of 2 mg coronene + 500 μL ethanol solution was drop-cast on the GCE/GMC surface, followed by drying the electrode in air at room temperature for 3 ± 1 min. Step 2: The modified electrode was potential-cycled in a window of -0.2 to 1.2 V vs Ag/AgCl at $\nu = 50$ mV s^{-1} for 20 continuous CV cycles in pH 7 PBS. Overall, 40 ± 2 min is required to prepare the GCE/GMC@Coronene-modified electrode.

■ ASSOCIATED CONTENT

Supporting Information

The Supporting Information is available free of charge at <https://pubs.acs.org/doi/10.1021/acsomega.0c01258>.

CV response of benzene solvent-purified coronene response on GCE/GMC-modified electrode in pH 2 KCl–HCl (Figure S1) (PDF)

■ AUTHOR INFORMATION

Corresponding Author

Annamalai Senthil Kumar – Nano and Bioelectrochemistry Research Laboratory, Department of Chemistry, School of Advanced Sciences and Carbon Dioxide Research and Green Technology Centre, Vellore Institute of Technology, Vellore 632014, India; orcid.org/0000-0001-8800-4038; Phone: +91-416-2202754; Email: askumarchem@yahoo.com, askumar@vit.ac.in

Author

Sivakumar Nisha – Nano and Bioelectrochemistry Research Laboratory, Department of Chemistry, School of Advanced Sciences, Vellore Institute of Technology, Vellore 632014, India

Complete contact information is available at: <https://pubs.acs.org/doi/10.1021/acsomega.0c01258>

Author Contributions

The manuscript was written through contributions of all authors. All authors have given approval to the final version of the manuscript.

Notes

The authors declare no competing financial interest.

■ ACKNOWLEDGMENTS

The authors acknowledge the Department of Science and Technology, Science and Engineering Research Board (DST-SERB-EMR/2016/002818) Scheme.

■ ABBREVIATIONS USED

GMC, graphitized mesoporous carbon; Cor, coronene; Cor-Redox, coronene redox system; SECM, scanning electrochemical microscope; GNP, graphite nanopowder; MWCNT, multiwalled carbon nanotube; SWCNT, single-walled carbon nanotube; CNF, carbon nanofiber

■ REFERENCES

(1) Mao, H. Y.; Laurent, S.; Chen, W.; Akhavan, O.; Imani, M.; Ashkarran, A. A.; Mahmoudi, M. Graphene: Promises, Facts,

Opportunities, and Challenges in Nanomedicine. *Chem. Rev.* **2013**, *113*, 3407–3424.

(2) Chee, W. K.; Lim, H. N.; Zainal, Z.; Huang, N. M.; Harrison, I.; Andou, Y. Flexible Graphene-Based Supercapacitors: A Review. *J. Phys. Chem. C* **2016**, *120*, 4153–4172.

(3) Whitener, K. E. Reversible Graphene Functionalization for Electronic Applications: A Review. *ACS Symp. Ser.* **2014**, *1183*, 41–54.

(4) Yuan, W.; Zhou, Y.; Li, Y.; Li, C.; Peng, H.; Zhang, J.; Liu, Z.; Dai, L.; Shi, G. The Edge-And Basal-Plane-Specific Electrochemistry of a Single-Layer Graphene Sheet. *Sci. Rep.* **2013**, *3*, No. 2248.

(5) Banks, C. E.; Davies, T. J.; Wildgoose, G. G.; Compton, R. G. Electrocatalysis at Graphite And Carbon Nanotube Modified Electrodes: Edge-Plane Sites And Tube Ends Are The Reactive Sites. *Chem. Commun.* **2005**, *7*, 829–841.

(6) Davies, T. J.; Hyde, M. E.; Compton, R. G. Nanotrench Arrays Reveal Insight into Graphite Electrochemistry. *Angew. Chem., Int. Ed.* **2005**, *32*, 5121–5126.

(7) Panda, S.; Rout, T. K.; Prusty, A. D.; Ajayan, P. M.; Nayak, S. Electron Transfer Directed Antibacterial Properties of Graphene Oxide On Metals. *Adv. Mater.* **2018**, *30*, No. 1702149.

(8) Hui, J.; Zhou, X.; Bhargava, R.; Chinderle, A.; Zhang, J.; Rodríguez-López, J. Kinetic Modulation of Outer-Sphere Electron Transfer Reactions on Graphene Electrode with A Sub-Surface Metal Substrate. *Electrochim. Acta* **2016**, *211*, 1016–1023.

(9) Jeong, D. W.; Park, S.; Choi, W. J.; Bae, G.; Chung, Y. J.; Yang, C. S.; Lee, Y. K.; Kim, J. J.; Park, N.; Lee, J. O. Electron-Transfer Transparency of Graphene: Fast Reduction of Metal Ions on Graphene-Covered Donor Surfaces. *Phys. Status Solidi RRL* **2015**, *9*, 180–186.

(10) Lee, J. U.; Lee, W.; Yoon, S. S.; Kim, J.; Byun, J. H. Site-Selective Immobilization of Gold Nanoparticles on Graphene Sheets and Its Electrochemical Properties. *Appl. Surf. Sci.* **2014**, *315*, 73–80.

(11) Amaro-Gahete, J.; Kaczmarek, A. M.; Esquivel, D.; Jiménez-Sanchidrián, C.; Van Der Voort, P.; Romero-Salguero, F. J. Luminescent Graphene-Based Materials Via Europium Complexation on Dipyridylpyridazine-Functionalized Graphene Sheets. *Chem. - Eur. J.* **2019**, *25*, 6823–6830.

(12) Urbanova, V.; Jayaramulu, K.; Schneemann, A.; Kment, S.; Fischer, R. A.; Zboril, R. Hierarchical Porous Fluorinated Graphene Oxide@ Metal–Organic Gel Composite: Label-Free Electrochemical Aptasensor for Selective Detection of Thrombin. *ACS Appl. Mater. Interfaces.* **2018**, *10*, 41089–41097.

(13) de la Torre, B.; Svec, M.; Hapala, P.; Redondo, J.; Krejci, O.; Lo, R.; Manna, D.; Sarmah, A.; Nachtigalova, D.; Tucek, J.; Blonski, P.; et al. Non-Covalent Control of Spin-State in Metal–Organic Complex by Positioning On N-Doped Graphene. *Nat. Commun.* **2018**, *9*, No. 2831.

(14) Liu, X.; Lee, E. K.; Oh, J. H. Graphene–Ruthenium Complex Hybrid Photodetectors with Ultrahigh Photoresponsivity. *Small* **2014**, *10*, 3700–3706.

(15) Zhang, X.; Bian, Y.; Sun, W.; Hu, T.; Liu, Y. Electronic and Magnetic Properties Regulation of Finite to Infinite Half Sandwich Organo-Transition-Metal-Complexes Functionalized Graphene. *RSC Adv.* **2016**, *6*, 97953–97960.

(16) Zhang, Z.; Turner, C. H. Redox properties of graphenes Functionalized with cyclopentadiene–transition metal complexes: A potential redox-active material. *J. Phys. Chem. C* **2014**, *118*, 24633–24640.

(17) Wang, H.; Rong, Q.; Ma, Z. Polyhydroquinone-Graphene Composite as New Redox Species for Sensitive Electrochemical Detection of Cytokeratins Antigen 21-1. *Sci. Rep.* **2016**, *6*, No. 30623.

(18) Xu, L.; Shi, R.; Li, H.; Han, C.; Wu, M.; Wong, C. P.; Kang, F.; Li, B. Pseudocapacitive Anthraquinone Modified with Reduced Graphene Oxide for Flexible Symmetric All-Solid-State Supercapacitors. *Carbon* **2018**, *127*, 459–468.

(19) Chen, D.; Tang, L.; Li, J. Graphene-based materials in electrochemistry. *Chem. Soc. Rev.* **2010**, *39*, 3157–3180.

(20) Kavan, L.; Dunsch, L. Spectroelectrochemistry of Carbon Nanotubes. *ChemPhysChem* **2011**, *12*, 47–55.

(21) Ambrosi, A.; Chua, C. K.; Latiff, N. M.; Loo, A. H.; An Wong, C. H.; Sheng Eng, A. Y.; Bonanni, A.; Pumera, M. Graphene and its Electrochemistry – an Update. *Chem. Soc. Rev.* **2016**, *45*, 2458–2493.

(22) Schulman, J. M.; Disch, R. L. Thermal and Magnetic Properties of Coronene and Related Molecules. *J. Phys. Chem. A* **1997**, *101*, 9176–9179.

(23) Jennings, E.; Montgomery, W.; Lerch, P. Stability of Coronene at high temperature and Pressure. *J. Phys. Chem. B* **2010**, *114*, 15753–15758.

(24) Frogley, B. J.; Wright, L. J. Cover Picture: A Metallaanthracene and Derived Metallaanthraquinone (*Angew. Chem. Int. Ed.* 1/2017). *Angew. Chem., Int. Ed.* **2017**, *56*, 1.

(25) Gingras, M.; Pinchart, A.; Dallier, C.; Mallah, T.; Levillain, E. Star-Shaped Nanomolecules Based on p-Phenylene Sulphide Asterisks with a Persulfurated Coronene Core. *Chem. - Eur. J.* **2004**, *10*, 2895–2904.

(26) Li, Z.; Smeu, M.; Rives, A.; Maraval, V.; Chauvin, R.; Ratner, M. A.; Borguet, E. Towards Graphyne Molecular Electronics. *Nat. Commun.* **2015**, *6*, No. 6321.

(27) Kawasaki, S.; Iwai, Y.; Hirose, M. Electrochemical Lithium Ion Storage Properties of Single-Walled Carbon Nanotubes Containing Organic Molecules. *Carbon* **2009**, *47*, 1081–1086.

(28) Zhang, R.; Zheng, H.; Shen, J. Blue Light-Emitting Diodes Based on Coronene-Doped Polymers. *Synth. Met.* **1999**, *105*, 49–53.

(29) Yeamin, M. B.; Faginas-Lago, N.; Albertí, M.; Cuesta, I. G.; Sanchez-Marin, J.; de Merás, A. S. Multi-Scale Theoretical Investigation of Molecular Hydrogen Adsorption Over Graphene: Coronene as a Case Study. *RSC Adv.* **2014**, *4*, 54447–54453.

(30) Morisset, S.; Rougeau, N.; Teillet-Billy, D. Influence of a Graphene Surface on the First Steps of the Hydrogenation of a Coronene Molecule. *Chem. Phys. Lett.* **2017**, *679*, 225–232.

(31) Saha, B.; Bhattacharyya, P. K. Anion- π Interaction in Oxoanion-Graphene Complex Using Coronene as Model System: A DFT Study. *Comput. Theor. Chem.* **2019**, *1147*, 62–71.

(32) Prodhon, S.; Mazumdar, S.; Ramasesha, S. Correlated Electronic Properties of a Graphene Nanoflake: Coronene. *Molecules* **2019**, *24*, 730.

(33) Jia, H. P.; Liu, S. X.; Sanguinet, L.; Levillain, E.; Decurtins, S. Star-Shaped Tetrathiafulvalene-Fused Coronene with Large π -Extended Conjugation. *J. Org. Chem.* **2009**, *74*, 5727–5729.

(34) Yoshida, Y.; Isomura, K.; Maesato, M.; Koretsune, T.; Nakano, Y.; Yamochi, H.; Kishida, H.; Saito, G. Cationic π -Stacking Columns of Coronene Molecules with Fully Charged and Charge-Disproportionated States. *Cryst. Growth Des.*, **2016**, *16*, 5994–6000.

(35) Yoshida, Y.; Maesato, M.; Kumagai, Y.; Mizuno, M.; Isomura, K.; Kishida, H.; Izumi, M.; Kubozono, Y.; Otsuka, A.; Yamochi, H.; Saito, G.; et al. Isotropic Three-Dimensional Molecular Conductor Based on The Coronene Radical Cation. *Eur. J. Inorg. Chem.* **2014**, *2014*, 3871–3878.

(36) Yoshida, Y.; Maesato, M.; Saito, G.; Kitagawa, H. Conducting Coronene Cation Radical Salt Containing Magnetic Metal Ions. *Inorg. Chem.* **2019**, *58*, 14068–14074.

(37) Chakrabarty, R.; Mukherjee, P. S.; Stang, P. J. Supramolecular Coordination: Self-Assembly of Finite Two-And Three-Dimensional Ensembles. *Chem. Rev.* **2011**, *111*, 6810–6918.

(38) Nisha, S.; Kumar, A. S. Electrochemical Conversion of Triamterene-Diuretic Drug to Hydroxybenzene-Triamterene Intermediate Mimicking the Pharmacokinetic Reaction on Multiwalled Carbon Nanotube Surface and Its Electrocatalytic Oxidation Function of Thiol. *J. Electroanal. Chem.* **2019**, *839*, 214–223.

(39) Bard, A. J.; Butler, J. N. Electroanalytical Chemistry. *J. Electrochem. Soc.*, **1967**, *114*, No. 5.

(40) Shen, Y.; Träuble, M.; Wittstock, G. Detection of Hydrogen Peroxide Produced During Electrochemical Oxygen Reduction Using Scanning Electrochemical Microscopy. *Anal. Chem.* **2008**, *80*, 750–759.

(41) Viswanathan, V.; Hansen, H. A.; Nørskov, J. K. Selective Electrochemical Generation of Hydrogen Peroxide from Water Oxidation. *J. Phys. Chem. Lett.* **2015**, *6*, 4224–4228.

(42) Bogan, B. W.; Lamar, R. T. One-Electron Oxidation in the Degradation of Creosote Polycyclic Aromatic Hydrocarbons by Phanerochaete Chrysosporium. *Appl. Environ. Microbiol.* **1995**, *61*, 2631–2635.

(43) Kim, P. M.; Deboni, U.; Wells, P. G. Peroxidase-Dependent Bioactivation and Oxidation of DNA and Protein in Benzo [a] Pyrene-Initiated Micronucleus Formation. *Free Radical Biol. Med.* **1997**, *23*, 579–596.

(44) Kumar, A. S.; Swetha, P. Simple Adsorption of Anthraquinone on Carbon Nanotube Modified Electrode and its Efficient Electrochemical Behaviors. *Colloids Surf., A* **2011**, *384*, 597–604.

(45) Barathi, P.; Kumar, A. S. Facile Electrochemical Oxidation of Polyaromatic Hydrocarbons to Surface-Confined Redox-Active Quinone Species on a Multiwalled Carbon Nanotube Surface. *Chem. Eur. J.* **2013**, *19*, 2236–2241.

(46) Günzler, H.; Gremlich, H. U. *IR Spectroscopy. An introduction*; Wiley-VCH: Weinheim, 2002.

(47) Lounasvuori, M. M.; Rosillo-Lopez, M.; Salzmann, C. G.; Caruana, D. J.; Holt, K. B. Electrochemical Characterisation of Graphene Nanoflakes with Functionalised edges. *Faraday Discuss.* **2014**, *172*, 293–310.

(48) Brownson, D. A.; Smith, G. C.; Banks, C. E. Graphene Oxide Electrochemistry: The Electrochemistry of Graphene Oxide Modified Electrodes Reveals Coverage Dependent Beneficial Electrocatalysis. *R. Soc. Open Sci.* **2017**, *4*, No. 171128.

(49) Bahceci, S.; Esat, B. A Polyacetylene Derivative with Pendant TEMPO Group as Cathode Material for Rechargeable Batteries. *J. Power Sources* **2013**, *242*, 33–40.

(50) Bindra, P.; Tweedie, J. Mechanisms of Electroless Metal Plating I. Application of the Mixed Potential Theory. *J. Electrochem. Soc.* **1983**, *130*, 1112–1114.

(51) Power, G. P.; Ritchie, I. M. Mixed Potential Measurements in the Elucidation of Corrosion Mechanisms—1. Introductory Theory. *Electrochim. Acta* **1981**, *26*, 1073–1078.

(52) Wang, Q.; Wang, S.; Shang, J.; Qiu, S.; Zhang, W.; Wu, X.; Li, J.; Chen, W.; Wang, X. Enhanced Electronic Communication and Electrochemical Sensitivity Benefiting from the Cooperation of Quadruple Hydrogen Bonding and π - π Interactions in Graphene/Multi-walled Carbon Nanotube Hybrids. *ACS Appl. Mater. Interfaces* **2017**, *9*, 6255–6264.

(53) Hammill, C. L.; Noble, B. B.; Norcott, P. L.; Ciampi, S.; Coote, M. L. Effect of Chemical Structure on the Electrochemical Cleavage of Alkoxyamines. *J. Phys. Chem. C* **2019**, *123*, 5273–5281.

(54) Reiche, S.; Blume, R.; Zhao, X. C.; Su, D.; Kunkes, E.; Behrens, M.; Schlögl, R. Reactivity of Mesoporous Carbon Against Water – An In-Situ XPS Study. *Carbon* **2014**, *77*, 175–183.

(55) Cañete-Rosales, P.; Ortega, V.; Alvarez-Luejea, A.; Bolloa, S.; Gonzálezb, M.; Ansónb, A.; Martínezb, M. T. Influence of Size and Oxidative Treatments of Multi-Walled Carbon Nanotubes on Their Electrocatalytic Properties. *Electrochim. Acta* **2012**, *62*, 163–171.

(56) Herrmann-Geppert, I.; Bogdanoff, P.; Radnik, J.; Fengler, S.; Dittrich, T.; Fiechter, S. Surface Aspects of Sol–Gel Derived Hematite Films for the Photoelectrochemical Oxidation of Water. *Phys. Chem. Chem. Phys.* **2013**, *15*, 1389–1398.

(57) Kumar, A. S.; Zen, J. M. Organic Redox Probes for The Key Oxidation States in Mixed Valence Ruthenium Oxide/Cyanometallate (Ruthenium Prussian Blue Analogue) Catalysts. *Electroanalysis* **2004**, *16*, 1211–1220.

(58) Kumar, A. S.; Sornambikai, S.; Venkatesan, S.; Chang, J. L.; Zen, J. M. Tetracycline Immobilization as Hydroquinone Derivative at Dissolved Oxygen Reduction Potential on Multiwalled Carbon Nanotube. *J. Electrochem. Soc.* **2012**, *159*, G137–G145.

(59) Lin, K. C.; Yin, C. Y.; Chen, S. M. An Electrochemical Biosensor for Determination of Hydrogen Peroxide Using Nanocomposite of Poly (methylene blue) and FAD Hybrid film. *Sens. Actuators, B* **2011**, *157*, 202–210.